

Supporting Information

Layer-controlled evolution of electron state in the silicene intercalation compound SrSi₂

*Oleg E. Parfenov, Alexander N. Taldenkov, Dmitry V. Averyanov, Ivan S. Sokolov,
Oleg A. Kondratev, Mikhail M. Borisov, Sergey N. Yakunin, Igor A. Karateev,
Andrey M. Tokmachev and Vyacheslav G. Storchak*

National Research Center “Kurchatov Institute”, Kurchatov Sq. 1, Moscow 123182, Russia

Contents:

Figure S1. Match of Si(111) and SrSi₂ lattices based on RHEED

Figure S2. XRD scans of ultrathin SrSi₂ films

Figure S3. Electron microscopy images of film interfaces

Figure S4. Electron microscopy images of ultrathin SrSi₂ films

Figure S5. Carrier mobilities and concentrations in SrSi₂

Figure S6. Independence of results on the electrical scheme

Figure S7. Weak antilocalization vs. chiral anomaly

Figure S8. Dependence of resistivity on out-of-plane rotation of magnetic field

Figure S9. Dependence of conductivity on in-plane rotation of magnetic field

Figure S10. Longitudinal magnetoconductance in 3 ML SrSi₂

Figure S11. Temperature dependence of resistivity for different thicknesses

Figure S12. Magnetoresistance of 8 ML SrSi₂

Figure S13. Magnetoresistance of 10 ML SrSi₂

Figure S14. Carrier mobilities and concentrations in 140 nm SrSi₂

Figure S15. Carrier mobilities and concentrations in 10 ML SrSi₂

Figure S16. Magnetoresistance of 30 nm SrSi₂

Figure S17. Interplay of weak localization and chiral anomaly

Figure S18. Two-terminal measurement scheme

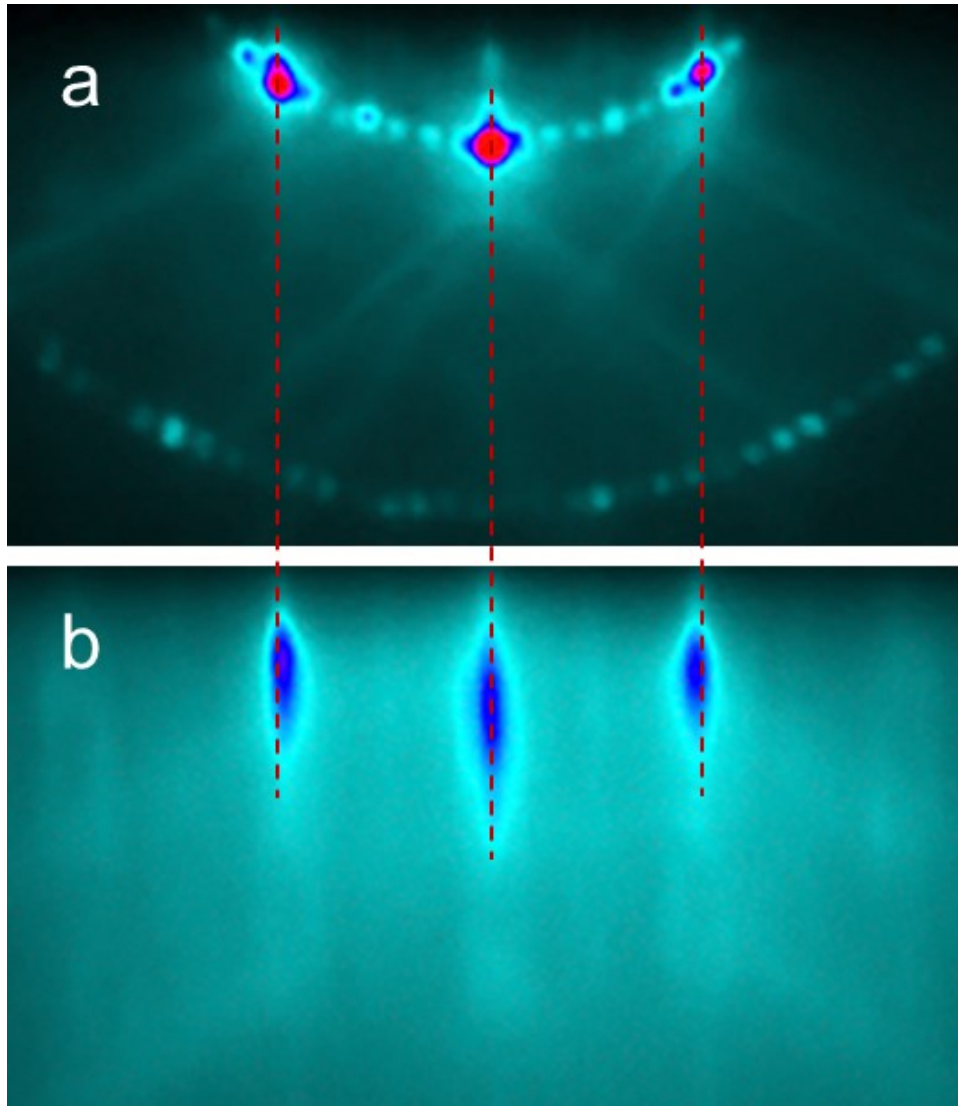


Figure S1. RHEED images along the $[1\bar{1}0]$ azimuth of the Si substrate. a) Reconstructed Si(111) surface. b) A film of SrSi₂ ($d = 160$ nm). The lattice match between the lateral lattice parameters of Si(111) and SrSi₂ is highlighted by red dashed lines.

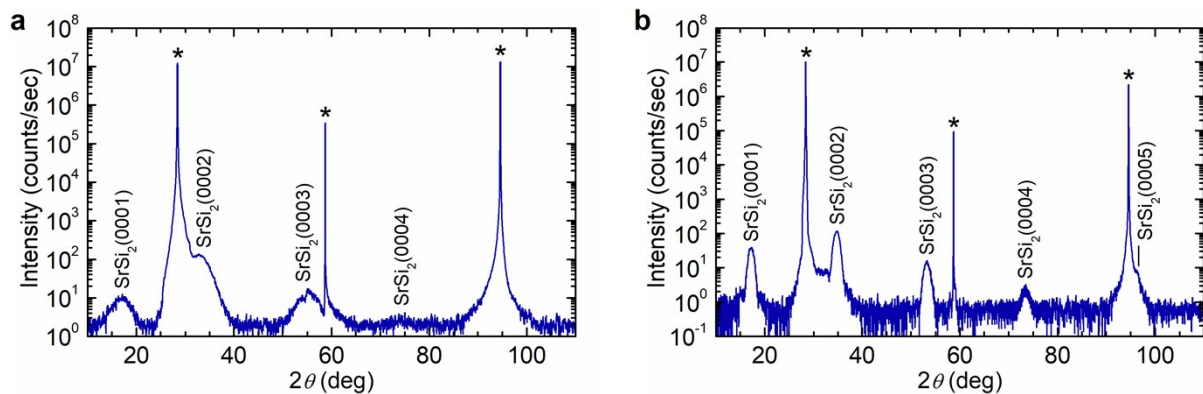


Figure S2. θ - 2θ XRD scans of ultrathin SrSi_2 films (the θ angles are scaled to the $\text{Cu K}\alpha_1$ wavelength to facilitate comparison with Fig. 1c): a) 3 ML and b) 8 ML; asterisks mark peaks from the substrate.

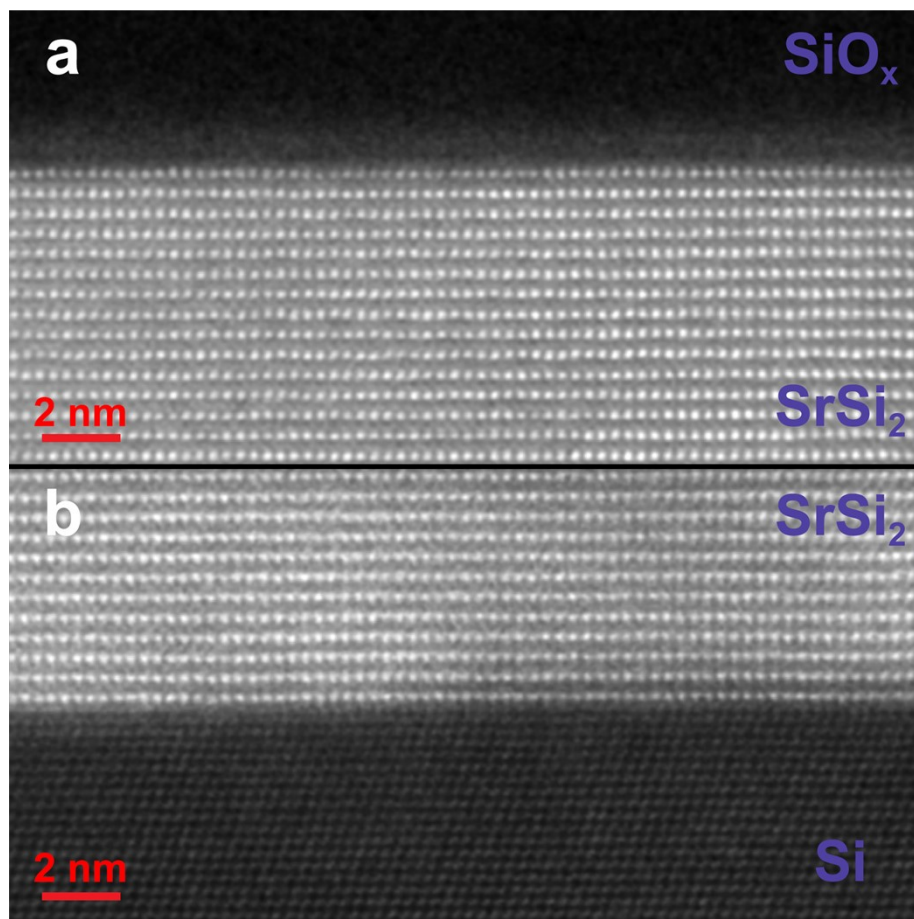


Figure S3. Cross-sectional HAADF-STEM images of interfaces in $\text{SiO}_x/\text{SrSi}_2/\text{Si}(111)$: a) the $\text{SiO}_x/\text{SrSi}_2$ interface; b) the $\text{SrSi}_2/\text{Si}(111)$ interface. Both images are viewed along the $[110]$ zone axis of the Si substrate.

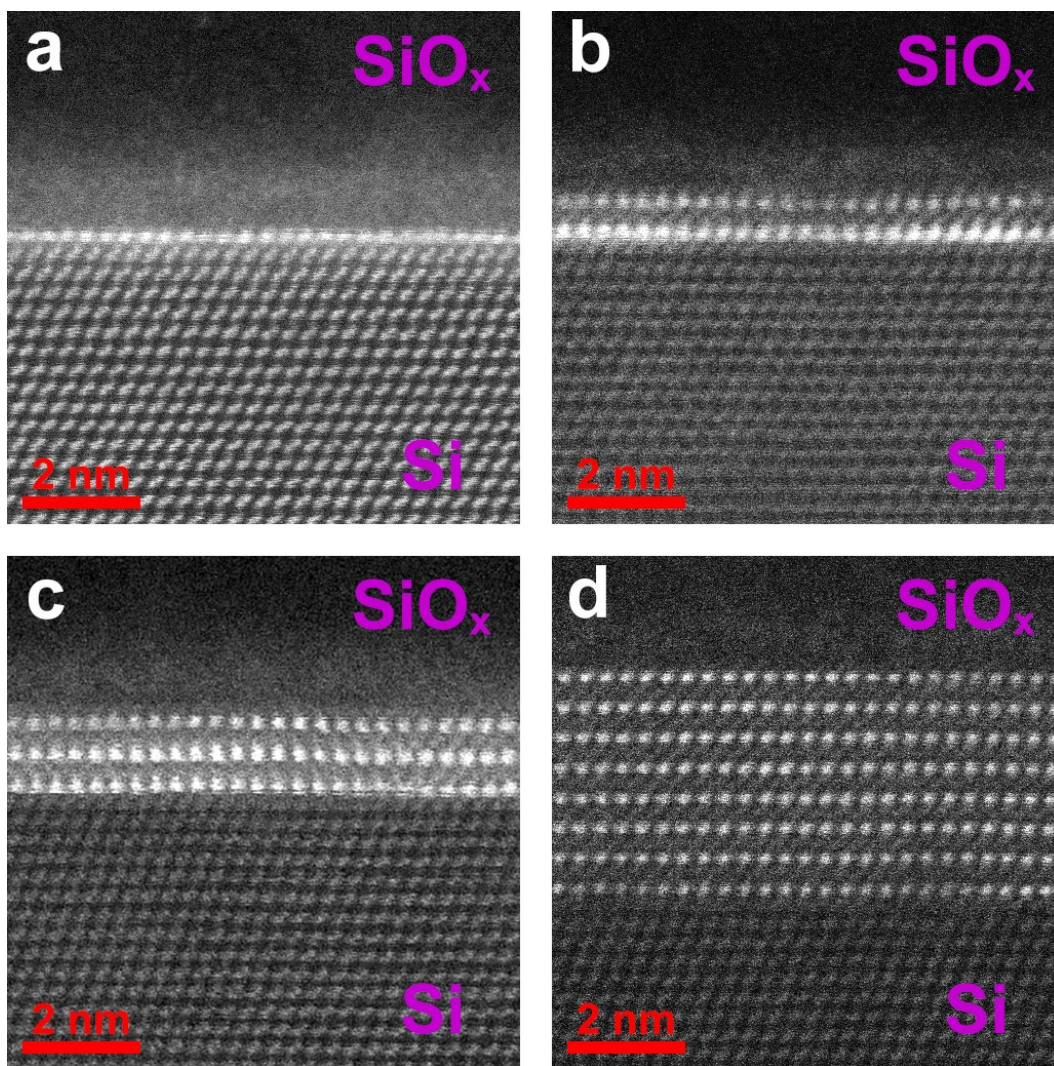


Figure S4. Cross-sectional HAADF-STEM images of ultrathin SrSi₂ films on Si(111): a) 1 ML; b) 2 ML; c) 3 ML; d) 8 ML. The images are viewed along the [110] zone axis of the Si substrate. Bright points correspond to Sr atoms.

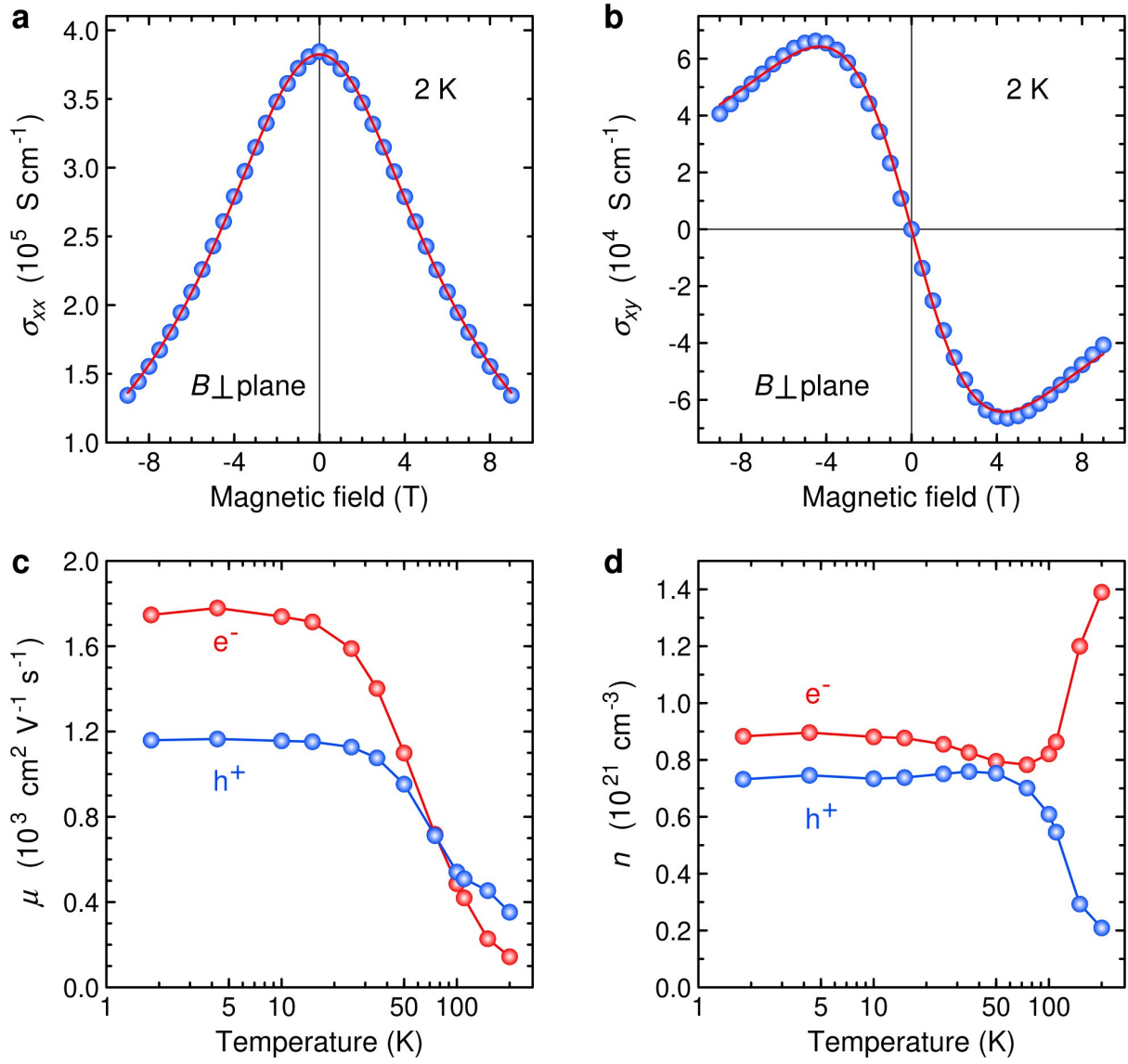


Figure S5. Electron transport in a thick SrSi₂ film ($d = 160 \text{ nm}$). a) Longitudinal and b) transverse conductance at 2 K in out-of-plane magnetic field; red lines provide fits of the data by a two-band model. Temperature dependence of c) carrier mobility and d) carrier concentration for the electron (red) and hole (blue) bands.

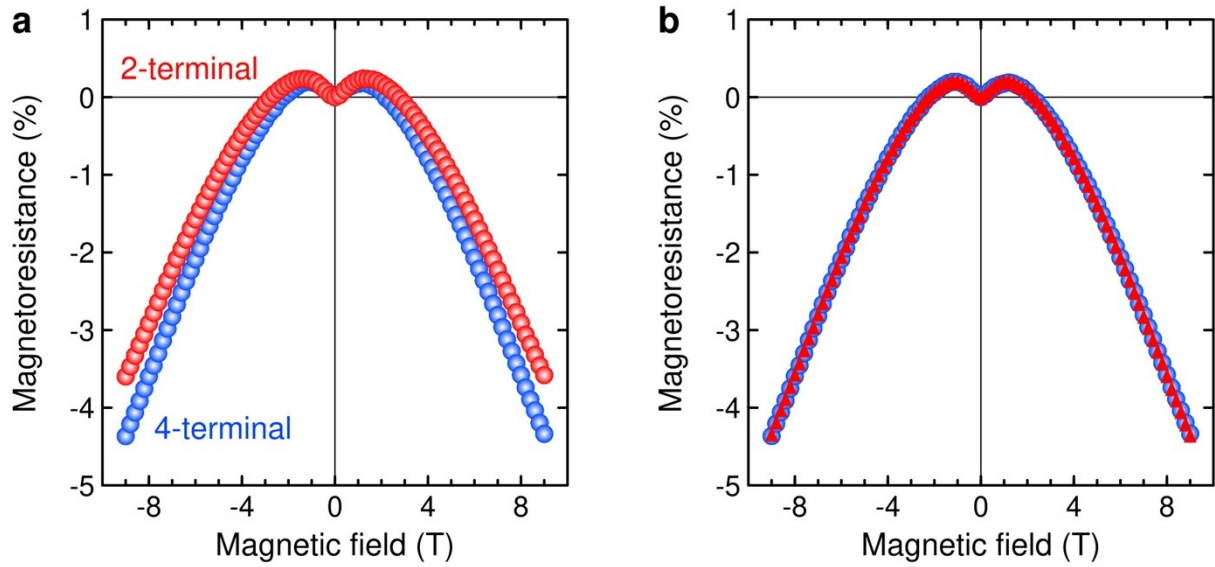


Figure S6. Electrical scheme dependence of magnetoresistance of a thick SrSi₂ film ($d = 160$ nm) at 2 K in magnetic field parallel to the current: a) 2-terminal (red) vs. 4-terminal (blue); b) interchange of potential and current contacts.

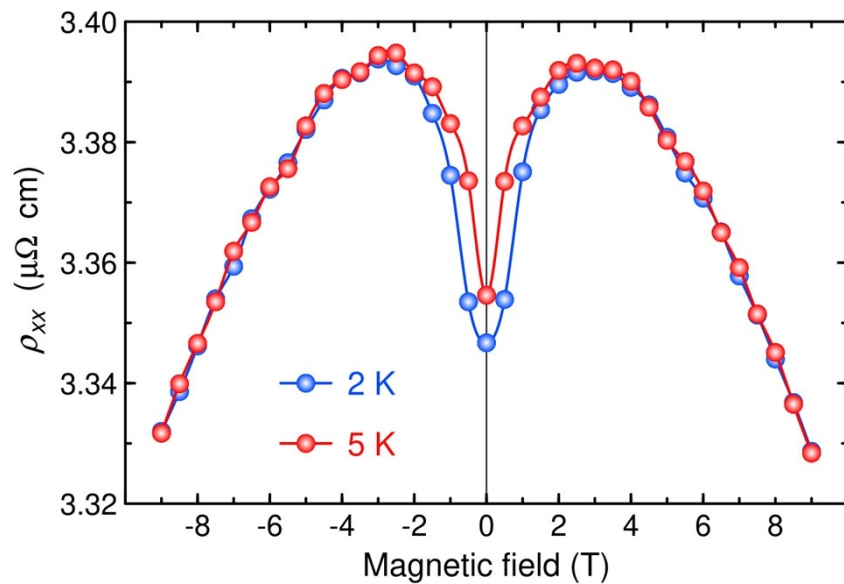


Figure S7. Resistivity of a thick SrSi₂ film ($d = 160$ nm) at $T = 2$ K (blue) and $T = 5$ K (red) in magnetic field parallel to the current.

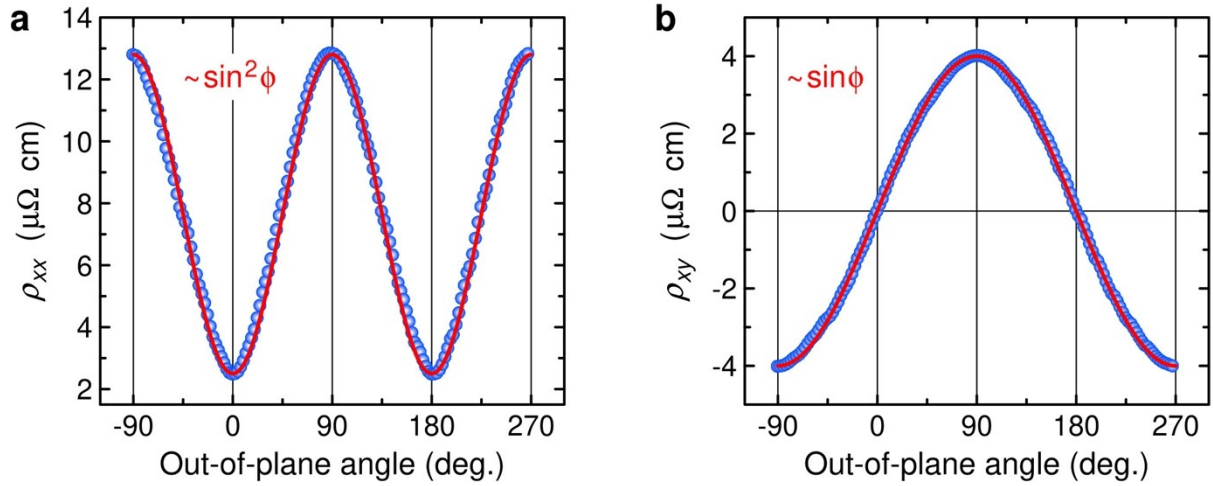


Figure S8. Dependence of a) longitudinal and b) transverse resistivity in a thick SrSi_2 film ($d = 160 \text{ nm}$) at $T = 2 \text{ K}$ on the angle ϕ between an out-of-plane magnetic field (with in-plane projection along the current direction) of 14 T and the current direction (blue dots) and their respective fits as $\text{const} \cdot \sin^2 \phi$ and $\text{const} \cdot \sin \phi$ (red lines).

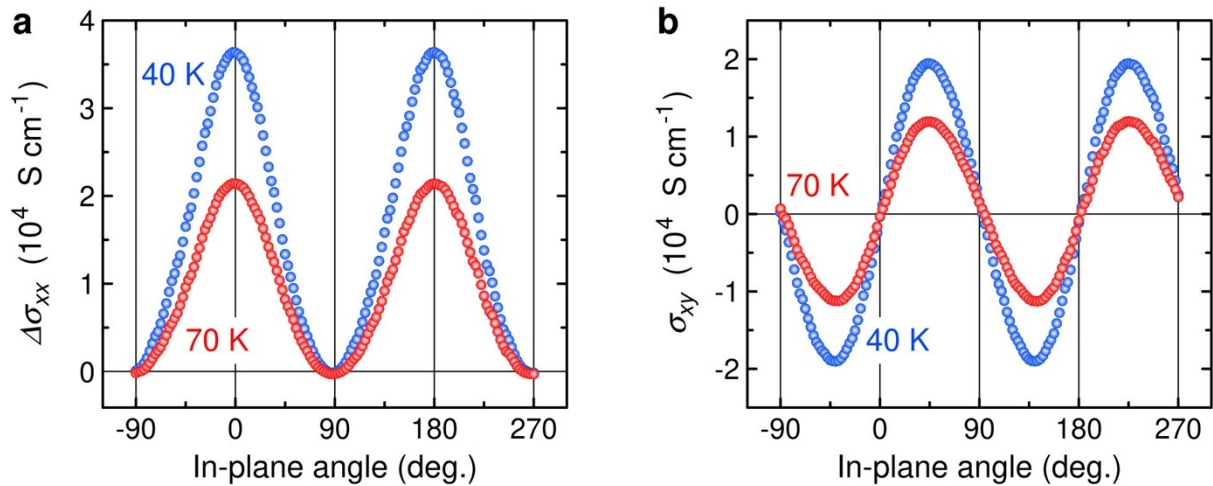


Figure S9. Dependence of a) longitudinal and b) transverse conductivity in a thick SrSi_2 film ($d = 160 \text{ nm}$) at 40 K (blue) and 70 K (red) on the angle θ between an in-plane magnetic field of 14 T and the current direction.

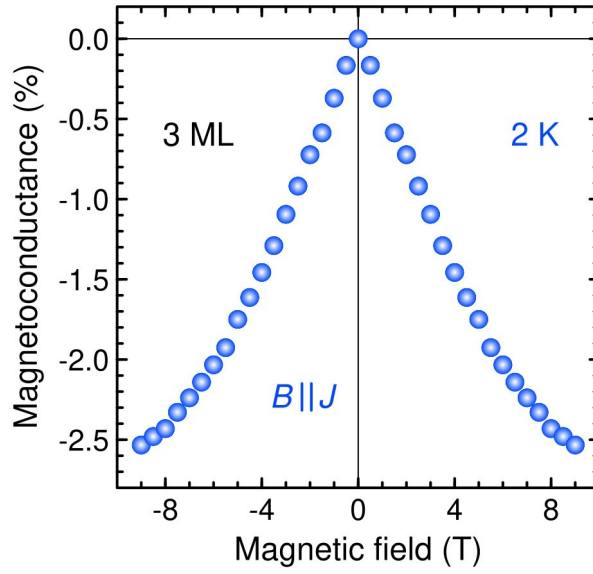


Figure S10. Magnetoconductance in 3 ML SrSi₂ at $T = 2$ K in magnetic field parallel to the current.

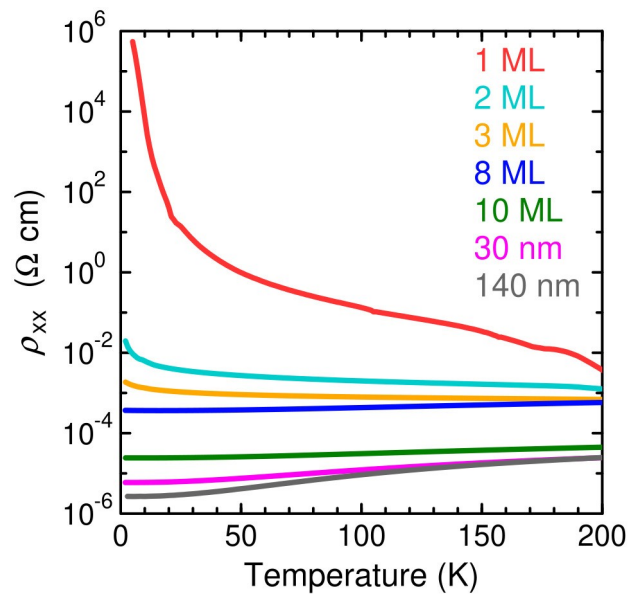


Figure S11. Temperature dependence of resistivity in SrSi₂ films of different thickness: 1 ML (red), 2 ML (cyan), 3 ML (orange), 8 ML (blue), 10 ML (green), 30 nm (magenta), and 140 nm (grey).

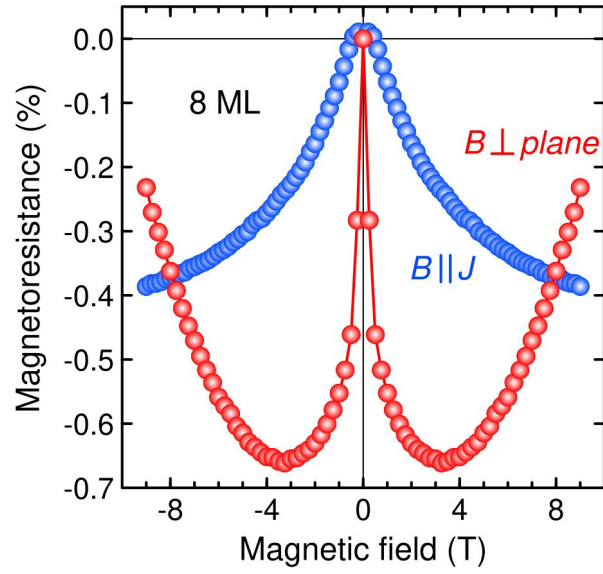


Figure S12. Magnetoresistance of 8 ML SrSi₂ at $T = 2$ K in magnetic fields directed in-plane (parallel to the current, blue) and out-of-plane (red).

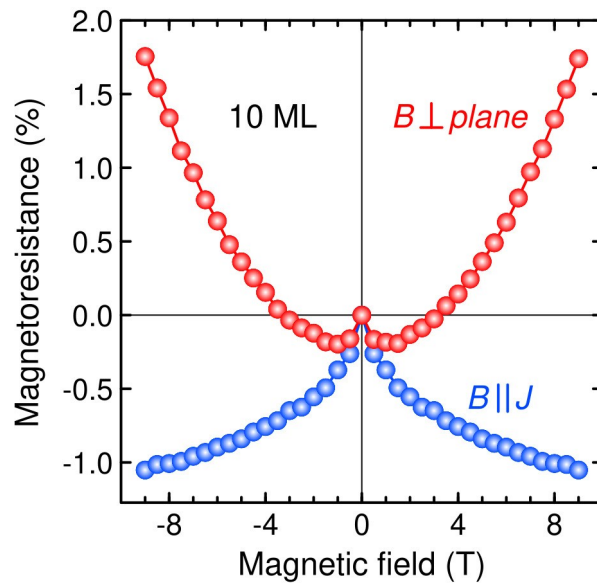


Figure S13. Magnetoresistance of 10 ML SrSi₂ at $T = 2$ K in magnetic fields directed in-plane (parallel to the current, blue) and out-of-plane (red).

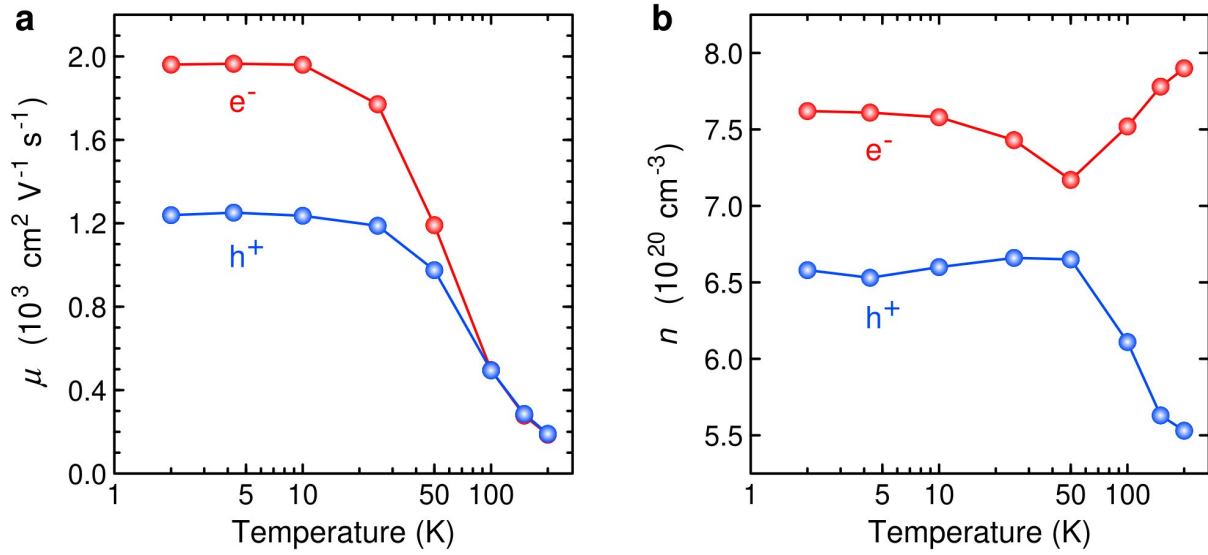


Figure S14. Temperature dependence of a) carrier mobility and b) carrier concentration for electrons (red) and holes (blue) in 140 nm SrSi₂.

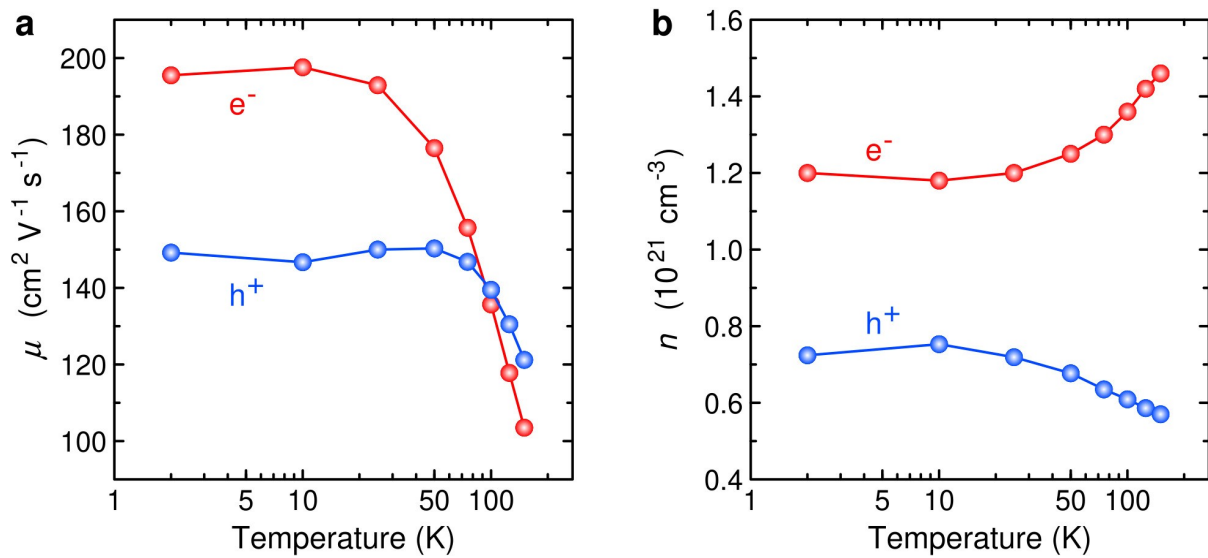


Figure S15. Temperature dependence of a) carrier mobility and b) carrier concentration for electrons (red) and holes (blue) in 10 ML SrSi₂.

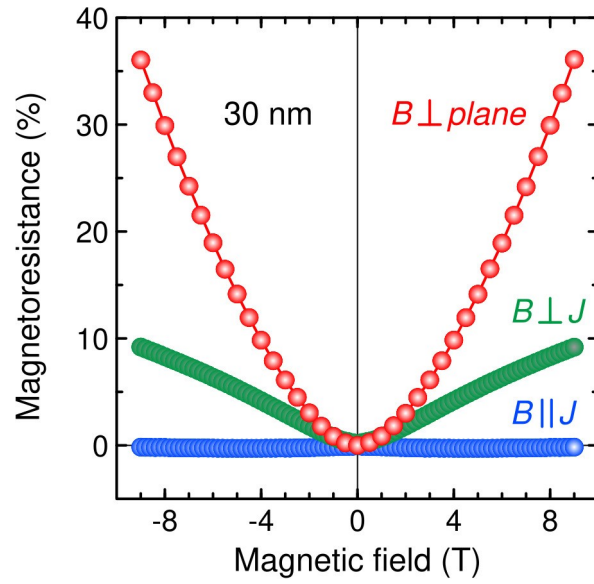


Figure S16. Magnetoresistance of 30 nm SrSi₂ at $T = 2$ K in in-plane magnetic field, parallel (blue) and orthogonal (green) to the current, and out-of-plane magnetic fields (red).

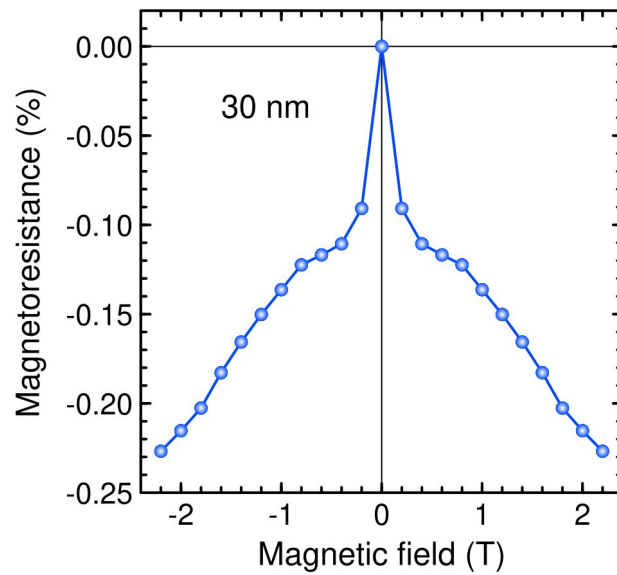


Figure S17. Magnetoresistance of a SrSi₂ film ($d = 30$ nm) at $T = 2$ K in magnetic field parallel to the current.

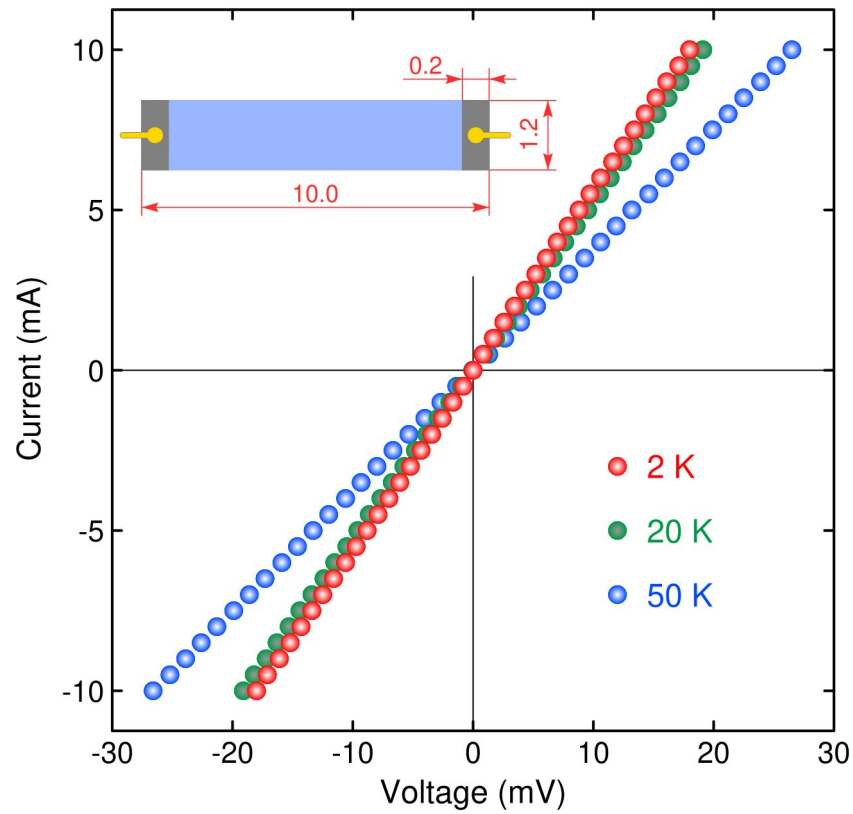


Figure S18. Two-terminal measurements of I-V characteristics in a thick SrSi₂ film ($d = 160$ nm) at 2 K (red), 20 K (green), and 50 K (blue) demonstrating an ohmic behavior. Inset shows a scheme of the measurements – the sample (blue) and the contact areas (grey); the distances are given in mm.